Mapping the niche of breast cancer metastases in lung and liver

Magdalena K. Sznurkowska[1], Francesc Castro-Giner[1], Yongzhan Zhang[1], Alexander Ring[1,2], Fabienne Dominique Schwab[3], Francesca Albrecht[3], Kirsten D. Mertz[4], Karin Strittmatter[1], Lauren L. Ozimski[1], Selina Budinjas[1], Gaël Auray[5], Claudio Giachino[5], Verdon Taylor[5], Ana Gvozdenovic[1], Ilaria Malanchi[6], Heike Frauchiger-Heuer[7], Andreas Wicki[2], Marcus Vetter[8] & Nicola Aceto[1,#]

[1] Department of Biology, Institute of Molecular Health Sciences, Swiss Federal Institute of Technology (ETH) Zurich, Zurich, Switzerland

[2] Department of Medical Oncology and Hematology, University Hospital Zurich and University of Zurich, Zurich, Switzerland

[3] Department of Gynecologic Oncology, University Hospital Basel and University of Basel, Basel, Switzerland

[4] Institute of Pathology, Cantonal Hospital Baselland, Liestal, Switzerland

[5] Department of Biomedicine, University of Basel, Basel, Switzerland

[6] The Francis Crick Institute, London, UK

[7] Department of Gynecologic Oncology, University Hospital Zurich, Zurich, Switzerland

[8] Cancer Center Baselland, Cantonal Hospital Baselland, Liestal, Switzerland

[#]Corresponding author: nicola.aceto@biol.ethz.ch

Abstract

Breast cancer progression to visceral organs such as lung and liver is regarded as a dreadful event, unequivocally associated with a poor prognosis. Yet, these vital sites are characterized by highly diverse cellular microenvironments and physiological functions, suggesting that they may influence cancer cells behavior in divergent ways. Unexpectedly, we find that while the liver microenvironment fosters metastasis-boosting properties of its metastatic seeds and favors secondary spread, the lungs impose a drastic roadblock to the same processes. Using patient data and mouse models of breast cancer that spontaneously metastasize to visceral organs, coupled with genetic barcode-mediated metastasis tracing, niche labeling technology and single cell analysis of both tumor cells and their direct microenvironment at each site, we characterize this dichotomy and identify differential microenvironmental factors that contribute to liver vs lung metastasis biology. Mechanistically, we uncover pulmonary cytokines, such as Granulin, whose activity naturally blocks metastatic properties. Conversely, we identify BMP2-producing endothelial cells within the liver metastatic niche, capable to enhance further spread. Together, we reveal an unexpected contrast in the site-specific behavior of visceral metastases in triple-negative breast cancer models, highlighting microenvironmental factors that contribute to its geographical diversity, as well as organ-specific opportunities for intervention.

Introduction

Metastasis is a major cause of cancer related deaths (*1*). While the newest emerging treatments are typically tested in patients with a metastatic disease, most of the underlying mechanistic insights that led to their unfolding derive from explorations of primary tumor biology (*2–4*). Consequently, little is known about how cancer cells are shaped at different anatomical sites during metastasis. A better understanding of cancer cells evolution as a function of their location is key to expose site-specific vulnerabilities and tailor new treatment interventions to a metastatic disease.

Breast cancer is the most common malignancy in women (*5*), and typically metastasizes to bone, liver, lungs and brain (*6*). The triple negative breast cancer (TNBC) subtype, defined by the lack of expression of HER2, estrogen and progesterone receptors (ER, PR), amounts to 10-15% of total breast cancers (*7*, *8*) and is characterized by an exceptionally aggressive phenotype, with poor outcome and limited treatment options compared to other subtypes (*7*, *8*). Intriguingly, TNBC spreads primarily to visceral organs, most commonly lungs and liver (*9*), in contrast to breast cancers of the ER positive subtype that display a more pronounced tropism for the bone (*10–13*). These metastatic patterns appear to affect disease outcome. For instance, the presence of bone metastases is associated with a more indolent disease and long-term outcomes, compared to other sites (*14*, *15*). On the other hand, reports on disease aggressiveness in the context of visceral metastases in the lungs and liver vary (*11*, *12*, *15*), yet, these two organs display substantially different anatomical and physiological features, suggesting that they could impact on cancer cells' biology in a different way.

Based on this, we hypothesized that lungs and liver shape breast cancer metastases in a divergent way, that the metastatic niche within these organs differs substantially, and that location has an impact on cancer cells development and progression-related features such as secondary seeding. We sought to uncover unique, site-specific biological changes that expose cancer cells to "geographical" vulnerabilities, paving the way to novel therapies that are designed not only based on general cancer-associated features, but also on metastasis location.

Results

Site-specific impact on survival

We first sought to determine whether differential metastatic patterns could affect patient survival. To this end, we examined the clinical history of 318 patients diagnosed with metastatic breast cancer between 1972 and 2019. Compared to most public cancer patient databases that collect recurrence data indirectly (*16*), our cohort contained direct diagnostic (metastatic) follow up information, allowing us to precisely define the metastatic progression sequence of each patient (table S1, S2). With the aim to assess whether metastasis to liver or lung could impact on survival in a different way, we focused on rare cases with mono-metastasis (n = 22, of which 10 were for the liver and 12 for the lung mono-metastases), whereby a single metastasis in lung or liver was present at the initial metastatic diagnosis (Fig. 1A). Of note, in this cohort, while liver and lung metastasis were generally prevalent (64.2% and 55.3%, respectively), the occurrence of a single, visceral metastasis as first metastatic diagnosis was noticeably rarer (3.8% for lung, 3.1% for liver). We found that patients with liver metastasis were characterized not only by a significantly shorter overall survival (log-rank P value = 0.016; hazard ratio (HR) = 3.2, 95% confidence interval (CI), 1.19 to 9.10),

consistently with a previous report (*11*), but also a shorter time to next metastatic event or death (log-rank *P* value = 0.001; HR=9.4, 95%CI, 1.88 to 46.88) compared to patients with lung metastases (Fig. 1B). Of note and in line with previous observations (*14*, *15*), metastases to the bone were associated with a better prognosis, similar to lung metastases (bone vs. liver : log-rank *P* value = 0.0004 and HR=0.23, 95%CI, 0.15 to 0.53; bone vs. lung: log-rank *P* value = 0.23 and HR=1.49, 95%CI, 0.78 to 2.86; fig. S1A,B). We then tested in an independent, external dataset from Surveillance, Epidemiology, and End Results Program (SEER), whether the presence of liver metastases of TNBC was also associated with a poorer prognosis compared to lung metastasis. Also in this case, we found that the time to next metastasis or death was longer for patients with initial lung metastasis diagnosis (fig. S1C) and that more of these patients had no cancer progression (metastasis or death) within 3 years of diagnosis compared to patients with liver metastasis diagnosis (fig. S1D). Altogether, these results highlight an unexpected impact on survival probability depending on whether the first visceral metastasis occurs in lungs or liver, suggesting an accelerated disease progression in breast cancer patients with liver metastases.

Clonal tracking of visceral metastases *in vivo*

We next sought to verify whether the correlation observed with the specific visceral site and disease aggressiveness could be attributed to the functional properties of the cells residing in the respective organs using a TNBC mouse model. To this end, we employed cellular barcoding, whereby triple negative MVT1 breast cancer cells were uniquely labelled with a genetic barcode library composed of 5 million barcodes. After barcoding, 100’000 breast cancer cells were injected orthotopically into the mammary fat pad of NSG female mice, mimicking physiological selection of the fittest clones as well as adaptation at target metastatic

124 sites. Of note, we purposely did not use immunocompetent syngeneic models for these
125 experiments, to avoid well-known immune system-mediated rejection of non-self
126 immunogenic components such as Cas9, fluorescence markers and genes conferring resistance
127 to substances with eukaryotic toxicity (*17*). Upon spontaneous metastasis to visceral sites, we
128 performed blood draw for circulating tumor cell (CTC) isolation as well as dissection of both
129 primary and metastatic sites, followed by targeted barcode sequencing to determine clonal
130 composition (Fig. 1C). Using a cutoff of 5 counts per million, we identified on average 11'091
131 barcodes in the primary tumor, 1'305 barcodes in CTCs, 918 and 1'094 barcodes in liver and
132 lung metastases, respectively (fig. S2A). We reasoned that the frequency and abundance of
133 barcodes unique to a particular metastatic site would reflect a limited ability to achieve
134 secondary seeding to new metastatic sites. We focused on unique barcodes in lungs and liver
135 with respect to all the other metastatic sites (fig. S2B-D). We observed that unique barcodes
136 were substantially more frequent in lungs compared to liver metastases (Fig. 1D,E, fig. S3A-
137 G). Alongside, compared to lung metastases, the barcode composition of liver metastases
138 exhibited higher similarity to CTCs (Fig. 1F, G, fig. S3H,I). Together, these results suggest a
139 differential behavior of TNBC cells as a function of their visceral metastatic site of residence,
140 whereby cells within liver metastases are encouraged to spread further, while cells within lung
141 metastases are far less likely to intravasate.
142

143 **The liver boosts, while the lungs suppress, metastatic properties of breast cancer cells**

144

145 Next, we set out to prospectively verify whether, beyond differential intravasation rates, cancer
146 cells that metastasized to liver or lungs would harbor a different ability to effectively achieve
147 secondary seeding. We employed orthotopic mammary fat pad injection of two TNBC cell
148 lines, MVT1 and 4T1, both lentivirally labelled with a GFP-luciferase construct. Upon tumor

149 growth and spontaneous dissemination to visceral sites, we isolated cancer cells that
150 metastasized to either lungs or liver and transplanted equal numbers (up to 15'000 cells each)
151 through the tail-vein of recipient, tumor-free NSG mice to measure metastatic outgrowth (Fig.
152 1H). In line with the higher spread, we found that liver-resident breast cancer cells gave rise to
153 significantly higher metastatic outgrowth in recipient mice compared to their lung-resident
154 counterpart (Fig. 1I-J). Altogether, these results not only suggest that liver-resident breast
155 cancer cells are characterized by higher shedding rates, but also that the liver microenvironment
156 enhances secondary metastasis-forming features of resident lesions, while the lung
157 microenvironment suppresses them.
158

159 **Organ-specific gene expression patterns of breast cancer cells**

160

161 To gain insights into the differential metastatic propensity of liver-resident vs lung-resident
162 breast cancer cells, we sought to investigate molecular features of both cancer cells and their
163 niche at each site at a single cell resolution. We first transduced GFP-labelled breast cancer
164 cells with a niche labelling system (*18*), allowing constitutive expression of a soluble mCherry
165 form that is taken up by neighboring cells, enabling prospective niche labeling upon
166 dissemination to lungs and liver. In this context, we isolated cancer (GFP-positive, mCherry-
167 positive) and niche (mCherry-positive) cells from the primary tumor, liver and lungs and
168 performed 10X single cell RNA sequencing (Fig. 2A). We first focused on the analysis of
169 28'105 cancer cells, of which 9'708 derived from the primary tumor, 9'442 derived from liver
170 metastases and 8'955 derived from lung metastases. When applying a uniform manifold
171 approximation and projection (UMAP) plot, we observed a clear separation of cancer cells as
172 a function of their location (Fig. 2B, C), alongside with the presence of gene expression clusters
173 specific to the primary tumor, liver, and lung metastases (Fig. 2D). Specifically, we observed

gene expression clusters 11 and 4 highly enriched within the primary tumor, clusters 7 and 12 specific to liver-resident metastases, and clusters 8 and 6 characteristic of lung-resident cancer cells. Based on this, we next investigated differentially expressed genes that characterize these clusters as well as each site, likely to reveal organ-specific gene expression dynamics of TNBC cancer cells. We adopted a pathway enrichment analysis strategy and pinpointed distinct gene sets upregulated in breast cancer cells resident in each organ (Fig. 2E) as well as within each of the gene expression clusters found to be most distinctive of the tumor-, liver- and lung-resident cells (Fig. 2F). As expected, we found high concordance between these two approaches. Pathways enriched within the primary tumor included a variety of gene sets related to translation, including eukaryotic translation initiation and formation of free 40S subunits. In contrast, liver-resident breast cancer cells displayed activity of a variety of metabolic processes related to energy generation, such as glycolysis, metabolism of carbohydrates, citric acid cycle and respiratory electron transport. All these shared a common feature of being related to ATP generation, consistent with a higher metastatic activity of liver-resident cells. On the other side, lung-resident breast cancer cells were enriched in processes such as apoptotic response or detoxification of reactive oxidative species, indicating a high degree of cellular stress (Fig. 2E, F, S4, table S3, 4). Together, these results reveal distinct molecular features of triple negative breast cancer cells as a function of their visceral organ of residence, suggesting that the tumor microenvironment shapes their biological features in an organ-dependent manner and raising an intriguing question regarding the identity and function of cells composing the metastatic niche in both liver and lungs.

198 **Interaction between breast cancer cells and their surrounding niche in liver and lungs**

199

200 We next shifted our focus to the niche component of the sequencing data (Fig. 3A), aiming to
201 pinpoint cell types – and their gene expression features – enriched in the tumor
202 microenvironment at different sites. To this end, we isolated, sequenced, and analyzed 12'558
203 niche cells, of which 4'257 microenvironment cells located within the primary tumor, 4'447
204 niche cells within liver metastases, and 3'854 niche cells within lung metastases. Interestingly,
205 we found substantial differences in the composition of the niche at different sites. For instance
206 myeloid cells, and in particular macrophages, are highly enriched within the microenvironment
207 of the primary tumor and lungs, yet they represent a much smaller fraction of the liver
208 metastatic niche (93% in primary tumor, 85% in lungs, 29% in liver) (Fig.3 B,C). When
209 comparing gene expression profiles of specific cell types of the niche at different locations, we
210 find particular features associated with primary tumor, liver and lung counterparts (fig. S5),
211 suggesting for instance the presence of alveolar macrophages within the lung niche and Kupfer
212 cells within the liver niche (fig. S5,6). Among the most striking differences, however, we found
213 the liver metastatic niche to be unique in respect to other locations, displaying a remarkable
214 enrichment in endothelial cells (Fig.3 B,C), suggesting a possible involvement of the
215 endothelium in shaping metastasis-forming features of liver-resident breast cancer cells.

216

217 We next sought to define key interactions between the cancer cells and different
218 components of their metastatic niche, focusing on surface receptors present on cancer cells and
219 corresponding ligands secreted by the niche counterpart, based on known and recognized
220 interaction pairs (*19*, *20*). For each ligand-receptor pair, we scored interactions using the
221 product of average ligand expression in niche cells and the average receptor expression across
222 all cancer cells. We selected interactions of significant score (P value < 0.05), and then

223 identified those that were present preferentially in liver or lungs (Fig. 3D, fig S7A,B), with a
224 ratio of at least 2-fold increase over the other counterpart. This enabled us to identify the lung-
225 specific macrophage cytokine-cancer receptor interactions of *Grn-Tnfrsf1a/b* and *Ssp1-Itgb1*.
226 For liver metastases we identified interactions between endothelial *Bmp2* cytokine and *Bmpr2*
227 and *Bmpr1a* cancer receptors, as well as endothelial *Bmp6* cytokine and *Bmpr2, Bmpr1a* and
228 *Acvr1* cancer receptors. The expression of ligands and receptors from selected interactions in
229 niche and cancer cells are depicted in Fig. 3E, showcasing a highly specific presence of *Bmp2*
230 and *Bmp6* cytokines in liver endothelial cells, as well as *Grn and Ssp1* expression in lung
231 macrophages (fig. 3E, fig. S7C). Together, these results highlight a different niche composition
232 for TNBC metastases in liver or lung, whereby the liver niche is enriched in endothelial cells
233 secreting *Bmp2* and *Bmp6* cytokines, while the lung niche is enriched in macrophages secreting
234 *Grn and Ssp1*.
235

236 **Niche-secreted cytokines modulate metastasis-forming properties of breast cancer cells**

237

238 With the purpose to validate our findings on liver and lung niche-specific cytokines and their
239 potential role in modulating the metastatic ability of resident breast cancer cells, we constructed
240 a minipool CRISPR Cas9 *in vivo* screen using MVT1-GFP-luciferase-Cas9 cells, designed to
241 target those receptors that are known to engage with the identified cytokines. Particularly, as
242 representatives of the liver niche we selected *Bmpr2* and *Bmpr1a* receptors that bind *Bmp2* and
243 *Bmp6* cytokines, as well as *Acvr1* that can partner with *Bmp6*. For pulmonary cytokines, we
244 selected *Tnfrsf1a/b* receptors that bind *Grn*, and *Itgb1* receptor that binds *Ssp1*. To identify
245 those receptors with metastasis promoting or suppressive function in different organs, we
246 performed a two-step *in vivo* experiment (Fig. 4A). First, the mutant cell pool was injected
247 intravenously into NSG mice, and upon metastasis establishment in lungs and liver, breast

248 cancer cells were isolated (referred to as lung- and liver-resident cells). We then performed
249 DNA extraction and targeted guide RNA (gRNA) sequencing to identify gene knockouts that
250 would provide cancer cells with direct metastatic advantages or disadvantages in primary
251 seeding to lungs or liver, or that would contribute to specific tropism patterns. In parallel, lung-
252 and liver-resident cells were re-injected into recipient tumor-free mice in equal numbers
253 (15'000 cells each) to model secondary seeding, and their metastatic spread was closely
254 monitored by means of bioluminescence imaging. At experiment termination, secondary liver
255 and lung metastases were isolated and profiled via targeted gRNA sequencing. This
256 experimental design enabled us to examine both the lung vs liver metastatic potential of
257 knockout cell pools, but also to test the requirement of each gene for secondary seeding, i.e.
258 after they have been exposed to the effects of the lung and liver niche.
259
260 Firstly, we observed a clear metastatic pattern of lung- and liver-resident cells when re-
261 injected in recipient mice, with their preferential tropism towards lung and liver metastases,
262 respectively, as well as a decrease in overall survival in mice injected with liver-resident cells
263 (Fig. 4B, C). Despite this, we could detect no significant difference in the abundance of specific
264 knockout cell clones between lung and liver-resident cells (*data not shown*), suggesting that
265 distinct tropism patterns and vulnerabilities could be primarily imposed on the knockout-cells
266 by the microenvironment at each site, while the longer-survival of mice injected with lung-
267 resident cells mice is consistent with the metastasis-suppressive role of the lung niche
268 demonstrated in Fig. 1. This lack of organ specific knockouts between lung- and liver-resident
269 cells could be due to the pleiotropic role of many of these receptors (*21–23*) and the existence
270 of interactions with additional cytokines beyond those indicated in Fig. 3D. Along these lines,
271 the expression of these receptors in cancer cells at the RNA level was similar in liver and lung
272 metastases (Fig. 3E). Yet, importantly, *Bmpr1a*-knockout cells (whereby *Bmpr1a* is the main

273 receptor for the liver niche-enriched *Bmp2* cytokine) were gradually depleted along the
274 experimental timeline, i.e. from pre-injection knockout pool control cells, through liver- and
275 lung- resident cells, to cells derived from lungs and livers of recipient mice (fig. S8). This
276 suggests an essential promoting role of this receptor in secondary metastasis and is consistent
277 with a previous report of its role in breast cancer progression (*24*). Conversely, *Tnfrsf1a*-
278 knockout cells (whereby *Tnfrsf1a* is the main receptor for the lung niche-enriched *granulin*
279 cytokine) were maintained throughout these conditions, indicating that this receptor does not
280 favor secondary seeding (fig. S8).
281
282 Based on these findings and trying to mimic the lung and liver niches, we then sought
283 to validate the impact of Granulin and Bmp2 on directly influencing new metastasis formation
284 (Fig 4D). To this end, we treated MVT1-GFP-luc cells *in vitro* with Granulin and BMP2
285 cytokines prior to their intravenous injection into tumor-free recipient mice, aiming to measure
286 direct, new metastasis seeding. In line with our CRISPR data, treatment with BMP2 led to an
287 enhanced metastatic ability of breast cancer cells, while Granulin treatment suppressed it (Fig.
288 4E). Altogether, these findings highlight that the liver and lung niches shape TNBC cells
289 differently through the action of selected cytokines. While on one hand, through the expression
290 of BMP2 by endothelial cells, the liver microenvironment boosts secondary seeding of lung-
291 resident metastases, on the other hand the expression of Granulin by macrophages within the
292 lung niche imposes a roadblock to further spread.
293

294 **Discussion**

295
296 A better understanding of the role of the niche cells within different metastatic sites in shaping
297 the properties of cancer cells is needed to better understand cancer cell biology as a function of

298 their location. This will shed light on processes that occur relatively late during a patient's
299 history, yet have a broad relevance for the development of new therapeutic options to be tested
300 for stage IV disease. Previously, it has been suggested that the bone metastatic niche may
301 invigorate cancer cells in bone metastasis models (*25*), a finding that is highly relevant for
302 hormone-driven cancers. Here, we provide first insights into the metastatic niche of lung and
303 liver metastases of TNBC. We observe unexpected differences in cellular composition, as well
304 as in the cytokine crosstalk between cancer and niche cells within these exclusive sites,
305 impacting on patterns of disease progression, metastasis-relevant characteristics, as well as
306 disease outcome.
307
308 We envision several scenarios that could benefit from these findings. For instance, on
309 the therapeutic angle, TNBC patients with liver or lung metastasis could be treated differently,
310 whereby patients with metastases localized exclusively to the liver (e.g. oligometastatic disease
311 to be treated with curative intent) could profit from BMP2 targeting alongside standard-of-care
312 treatments, aiming to interfere with secondary metastasis formation. Conversely, stimulating
313 the action of Granulin could result in a constitutive inhibition of TNBC spread, mimicking the
314 lung microenvironment.
315
316 Although our study focused on TNBC given its marked propensity to metastasize to
317 visceral sites, many other cancer types do spread to liver and lungs. The question of whether
318 our findings on the niche composition on these sites as well as the changes that occur in liver-
319 resident vs lung-resident TNBC cells also occur in other cancer types with similar metastatic
320 patterns remains unanswered. Uncovering this unexpected dichotomy for sites that have been
321 associated with TNBC should stimulate further investigations in this context, aimed to better

map metastatic behaviors, biology and vulnerabilities not only from a generic cancer cell perspective, but also from a geographical standpoint.

Figure Legends

Figure 1. Metastatic ability of liver-resident *versus* lung-resident TNBC cells.

A. Schematic showcasing the concept behind patient data analysis. **B.** Kaplan-Meier plots depicting time to next metastasis or death (*left*) and overall survival (*right*) of breast cancer patients with the first mono-metastatic event detected in lungs (n=12) or liver (n=10). **C.** Schematic representing the experimental design for barcode labelling and metastasis clonality assessment in NSG mice carrying MVT1-GFP-luciferase tumors. **D.** Volcano plot illustrating unique barcodes for lung and liver metastases of a representative mouse. **E.** Pie charts showing the percent of unique barcodes detected in lungs or liver metastases (*top*), as well as the unique barcode contribution to metastasis in lungs and liver (*bottom*). **F.** Principal component analysis (PCA) plot of 500 top variable barcodes represented in the primary tumor (PT), circulating tumor cells (CTCs), lung and liver metastases of a representative mouse. **G.** Dot plot showing Euclidean distances measuring the dissimilarity in barcode expression between lung or liver metastases and CTCs (n=3mice). ****, $P < 0.0001$ by Mann-Whitney test. **H.** Illustration of the experimental design for metastatic potential assessment of lung- and liver-resident cancer cells. **I-J.** Representative images (*left*) and quantification (*right*) of bioluminescent signals in indicated organs of animals injected with lung- and liver-resident MVT1-GFP-luciferase (**I**, n=9 mice per group) and 4T1-GFP-luciferase cells (**J,** n=11,8 mice per lung-, liver-derived groups, respectively). **, $P < 0.01$ by Mann-Whitney test. IV, intravenous; BLI, bioluminescence imaging.

347 **Figure 2. Liver-resident and lung-resident breast cancer cells display distinct molecular**
348 **profiles.**
349 **A.** Overview of the niche-labelling experiment with MVT1-GFP-luciferase xenografts with a
350 specific focus on cancer cells. **B-C.** Uniform Manifold Approximation and Projection (UMAP)
351 embedding colored by **B)** organ of origin and **C)** gene expression cluster number. **D.** Box-plot
352 representation of specific gene expression clusters enriched within the primary tumor (PT),
353 liver and lung metastases, along with associated abundances at each anatomical site (propeller
354 derived adjusted *P* value; *, $P < 0.05$; **, $P < 0.01$; ***, $P < 0.001$; ****, $P < 0.0001$). **E-F.**
355 Enriched reactome pathways in **E)** organ specific gene expression clusters and in **F)** all cancer
356 cells associated with a given organ. Top 10 pathways for each group with hypergeometric test
357 adjusted $P < 0.01$ are shown. Displayed is a condensed set of ontologies following
358 simplification through semantic similarity. The complete pathway list is provided in tables S3
359 and S4.
360
361 **Figure 3. Metastatic niche composition of liver and lungs in TNBC.**
362 **A.** Overview of the niche-labelling experiment with MVT1-GFP-luciferase xenografts with a
363 specific focus on metastatic niche cells. **B.** Uniform Manifold Approximation and Projection
364 (UMAP) embedding of niche cells colored by organ. Annotations indicate the locations of
365 estimated cell types within UMAP. **C.** Pie charts displaying cell type distributions within the
366 primary tumor (PT) and the metastatic niches of liver and lungs. **D.** Dot plot representing
367 selected interactions between cytokine ligands (niche cells) and their receptors (cancer cells).
368 Dot color and size correspond to the average interaction score scaled for each ligand-receptor
369 pair using minimum-maximum normalization. **E.** UMAP displaying cytokine and receptor
370 expression in niche cells and cancer cells, respectively (refer to panel **B** and **Fig. 2B** for the cell
371 type and organ of origin).

372 **Figure 4. Niche-secreted cytokine impact on metastatic properties of lung-resident and**
373 **liver-resident TNBC cells.**
374 **A.** Illustration of the *in vivo* loss of function minipool CRISPR Cas9 screen designed to
375 investigate the role of selected cytokine-receptor pairs using MVT1-GFP-luciferase xenografts.
376 **B.** Representative images of livers and lungs from animals re-transplanted with lung- or liver-
377 resident cancer cells. GFP signal (*green*) demarcates the presences of cancer cells. Scale bars,
378 500µm. **C.** Kaplan-Meier curve showing the survival of mice re-injected with either lung- or
379 liver-resident cancer cells. $P = 0.0012$ by log-rank test. **D.** Experimental design to explore the
380 role of selected niche-specific cytokines in metastasis formation. **E.** Representative images
381 (*left*) and quantification (*right*) of bioluminescence signals of lungs in animals injected with
382 BMP2 and Granulin (GRN) treated cells. **, $P < 0.01$ by Mann-Whitney test. IV, intravenous;
383 BLI, bioluminescence imaging.
384
385

386 ## Acknowledgments

387

388 We thank members and collaborators of the Aceto Laboratory for scientific feedback and
389 discussions. We thank the Functional Genomic Center Zurich for generating libraries and
390 carrying out next-generation sequencing; the Flow Cytometry Core facility (ETH Zurich) for
391 assistance with FACS-based experiments; A.Offinger (University of Basel) and her team as
392 well as the EPIC team (ETH Zurich) for support with animal work. The Aceto laboratory is
393 supported by the European Research Council (101001652), the strategic focus area of
394 personalized health and related technologies at ETH Zurich (PHRT-541 and PHRT-960), the
395 Swiss National Science Foundation (212183), the Swiss Cancer League (KLS-5636-08-2022),
396 the ETH Lymphoma Challenge (LC-02-22) and ETH Zurich. M.K. Sznurkowska is a H2020

Marie Skłodowska-Curie Actions (847012) and an EMBO Long Term Fellow (ALTF 899-2018).

Author contributions

M.K.S. and N.A. designed the study. M.K.S performed all experiments. F.C.G performed all computational analyses and Y.Z performed barcode computational analysis. A.R., F.D.S, F.A. and K.D.M. collected clinical data. S.B., K.S., L.L.O., C.G., and G.A. assisted with experiments. V.T. supervised some experiments. I.M. provided the construct for niche-labelling. H.F.H. A.W. and M.V. supervised clinical data acquisition. M.K.S, A.G. and N.A. wrote the manuscript. All authors read the manuscript and provided feedback.

Competing interests

N.A. is a co-founder and member of the board of PAGE Therapeutics AG, Switzerland, listed as an inventor in patent applications related to CTCs, a paid consultant for companies with an interest in liquid biopsies, and a Novartis shareholder.

421 **References**

422

423 1. H. Dillekås, M. S. Rogers, O. Straume, Are 90% of deaths from cancer caused by
424 metastases? *Cancer Medicine* **8**, 5574–5576 (2019).

425 2. P. Gui, T. G. Bivona, Evolution of metastasis: new tools and insights. *Trends in Cancer*
426 **8**, 98–109 (2022).

427 3. A. L. Parker, M. Benguigui, J. Fornetti, E. Goddard, S. Lucotti, J. Insua-Rodríguez, A. P.
428 Wiegmans, Early Career Leadership Council of the Metastasis Research Society, Current
429 challenges in metastasis research and future innovation for clinical translation. *Clin Exp*
430 *Metastasis* **39**, 263–277 (2022).

431 4. A. A. Abdul Pari, M. Singhal, H. G. Augustin, Emerging paradigms in metastasis
432 research. *Journal of Experimental Medicine* **218**, e20190218 (2021).

433 5. H. Sung, J. Ferlay, R. L. Siegel, M. Laversanne, I. Soerjomataram, A. Jemal, F. Bray,
434 Global Cancer Statistics 2020: GLOBOCAN Estimates of Incidence and Mortality
435 Worldwide for 36 Cancers in 185 Countries. *CA A Cancer J Clinicians* **71**, 209–249
436 (2021).

437 6. H. Kennecke, R. Yerushalmi, R. Woods, M. C. U. Cheang, D. Voduc, C. H. Speers, T. O.
438 Nielsen, K. Gelmon, Metastatic Behavior of Breast Cancer Subtypes. *JCO* **28**, 3271–
439 3277 (2010).

440 7. P. Zagami, L. A. Carey, Triple negative breast cancer: Pitfalls and progress. *npj Breast*
441 *Cancer* **8**, 95 (2022).

442 8. K. H. Allison, M. E. H. Hammond, M. Dowsett, S. E. McKernin, L. A. Carey, P. L.
443 Fitzgibbons, D. F. Hayes, S. R. Lakhani, M. Chavez-MacGregor, J. Perlmutter, C. M.
444 Perou, M. M. Regan, D. L. Rimm, W. F. Symmans, E. E. Torlakovic, L. Varella, G.
445 Viale, T. F. Weisberg, L. M. McShane, A. C. Wolff, Estrogen and Progesterone Receptor
446 Testing in Breast Cancer: American Society of Clinical Oncology/College of American
447 Pathologists Guideline Update. *Archives of Pathology & Laboratory Medicine* **144**, 545–
448 563 (2020).

449 9. Q. Wu, J. Li, S. Zhu, J. Wu, C. Chen, Q. Liu, W. Wei, Y. Zhang, S. Sun, Breast cancer
450 subtypes predict the preferential site of distant metastases: a SEER based study.
451 *Oncotarget* **8**, 27990–27996 (2017).

452 10. H. Zhao, Y. Gong, F. Ye, H. Ling, X. Hu, Incidence and prognostic factors of patients
453 with synchronous liver metastases upon initial diagnosis of breast cancer: a population-
454 based study. *CMAR* **Volume 10**, 5937–5950 (2018).

455 11. L. Gerratana, V. Fanotto, M. Bonotto, S. Bolzonello, A. M. Minisini, G. Fasola, F.
456 Puglisi, Pattern of metastasis and outcome in patients with breast cancer. *Clin Exp*
457 *Metastasis* **32**, 125–133 (2015).

12. W. Xiao, S. Zheng, P. Liu, Y. Zou, X. Xie, P. Yu, H. Tang, X. Xie, Risk factors and survival outcomes in patients with breast cancer and lung metastasis: a population-based study. *Cancer Med* **7**, 922–930 (2018).

13. H. Pan, R. Gray, J. Braybrooke, C. Davies, C. Taylor, P. McGale, R. Peto, K. I. Pritchard, J. Bergh, M. Dowsett, D. F. Hayes, 20-Year Risks of Breast-Cancer Recurrence after Stopping Endocrine Therapy at 5 Years. *N Engl J Med* **377**, 1836–1846 (2017).

14. S. J. Lee, S. Park, H. K. Ahn, J. H. Yi, E. Y. Cho, J. M. Sun, J. E. Lee, S. J. Nam, J.-H. Yang, Y. H. Park, J. S. Ahn, Y.-H. Im, Implications of Bone-Only Metastases in Breast Cancer: Favorable Preference with Excellent Outcomes of Hormone Receptor Positive Breast Cancer. *Cancer Res Treat* **43**, 89–95 (2011).

15. R. Wang, Y. Zhu, X. Liu, X. Liao, J. He, L. Niu, The Clinicopathological features and survival outcomes of patients with different metastatic sites in stage IV breast cancer. *BMC Cancer* **19**, 1091 (2019).

16. J. L. Warren, A. Mariotto, D. Melbert, D. Schrag, P. Doria-Rose, D. Penson, K. R. Yabroff, Sensitivity of Medicare Claims to Identify Cancer Recurrence in Elderly Colorectal and Breast Cancer Patients. *Medical Care* **54**, e47–e54 (2016).

17. C. A. Grzelak, E. T. Goddard, E. E. Lederer, K. Rajaram, J. Dai, R. E. Shor, A. R. Lim, J. Kim, S. Beronja, A. P. W. Funnell, C. M. Ghajar, Elimination of fluorescent protein immunogenicity permits modeling of metastasis in immune-competent settings. *Cancer Cell* **40**, 1–2 (2022).

18. L. Ombrato, E. Nolan, I. Kurelac, A. Mavousian, V. L. Bridgeman, I. Heinze, P. Chakravarty, S. Horswell, E. Gonzalez-Gualda, G. Matacchione, A. Weston, J. Kirkpatrick, E. Husain, V. Speirs, L. Collinson, A. Ori, J.-H. Lee, I. Malanchi, Metastatic-niche labelling reveals parenchymal cells with stem features. *Nature* **572**, 603–608 (2019).

19. S. Cabello-Aguilar, M. Alame, F. Kon-Sun-Tack, C. Fau, M. Lacroix, J. Colinge, SingleCellSignalR: inference of intercellular networks from single-cell transcriptomics. *Nucleic Acids Research* **48**, e55–e55 (2020).

20. L. Garcia-Alonso, L.-F. Handfield, K. Roberts, K. Nikolakopoulou, R. C. Fernando, L. Gardner, B. Woodhams, A. Arutyunyan, K. Polanski, R. Hoo, C. Sancho-Serra, T. Li, K. Kwakwa, E. Tuck, V. Lorenzi, H. Massalha, M. Prete, V. Kleshchevnikov, A. Tarkowska, T. Porter, C. I. Mazzeo, S. Van Dongen, M. Dabrowska, V. Vaskivskyi, K. T. Mahbubani, J. Park, M. Jimenez-Linan, L. Campos, V. Yu. Kiselev, C. Lindskog, P. Ayuk, E. Prigmore, M. R. Stratton, K. Saeb-Parsy, A. Moffett, L. Moore, O. A. Bayraktar, S. A. Teichmann, M. Y. Turco, R. Vento-Tormo, Mapping the temporal and spatial dynamics of the human endometrium in vivo and in vitro. *Nat Genet* **53**, 1698–1711 (2021).

21. Valer, Sánchez-de-Diego, Pimenta-Lopes, Rosa, Ventura, ACVR1 Function in Health and Disease. *Cells* **8**, 1366 (2019).

22. M.-J. Kim, S. Y. Park, H. R. Chang, E. Y. Jung, A. Munkhjargal, J.-S. Lim, M.-S. Lee, Y. Kim, Clinical significance linked to functional defects in bone morphogenetic protein type 2 receptor, BMPR2. *BMB Rep.* **50**, 308–317 (2017).

23. P. Gough, I. A. Myles, Tumor Necrosis Factor Receptors: Pleiotropic Signaling Complexes and Their Differential Effects. *Front. Immunol.* **11**, 585880 (2020).

24. M. W. Pickup, L. D. Hover, Y. Guo, A. E. Gorska, A. Chytil, S. V. Novitskiy, H. L. Moses, P. Owens, Deletion of the BMP receptor BMPR1a impairs mammary tumor formation and metastasis. *Oncotarget* **6**, 22890–22904 (2015).

25. W. Zhang, I. L. Bado, J. Hu, Y.-W. Wan, L. Wu, H. Wang, Y. Gao, H.-H. Jeong, Z. Xu, X. Hao, B. M. Lege, R. Al-Ouran, L. Li, J. Li, L. Yu, S. Singh, H. C. Lo, M. Niu, J. Liu, W. Jiang, Y. Li, S. T. C. Wong, C. Cheng, Z. Liu, X. H.-F. Zhang, The bone microenvironment invigorates metastatic seeds for further dissemination. *Cell* **184**, 2471-2486.e20 (2021).

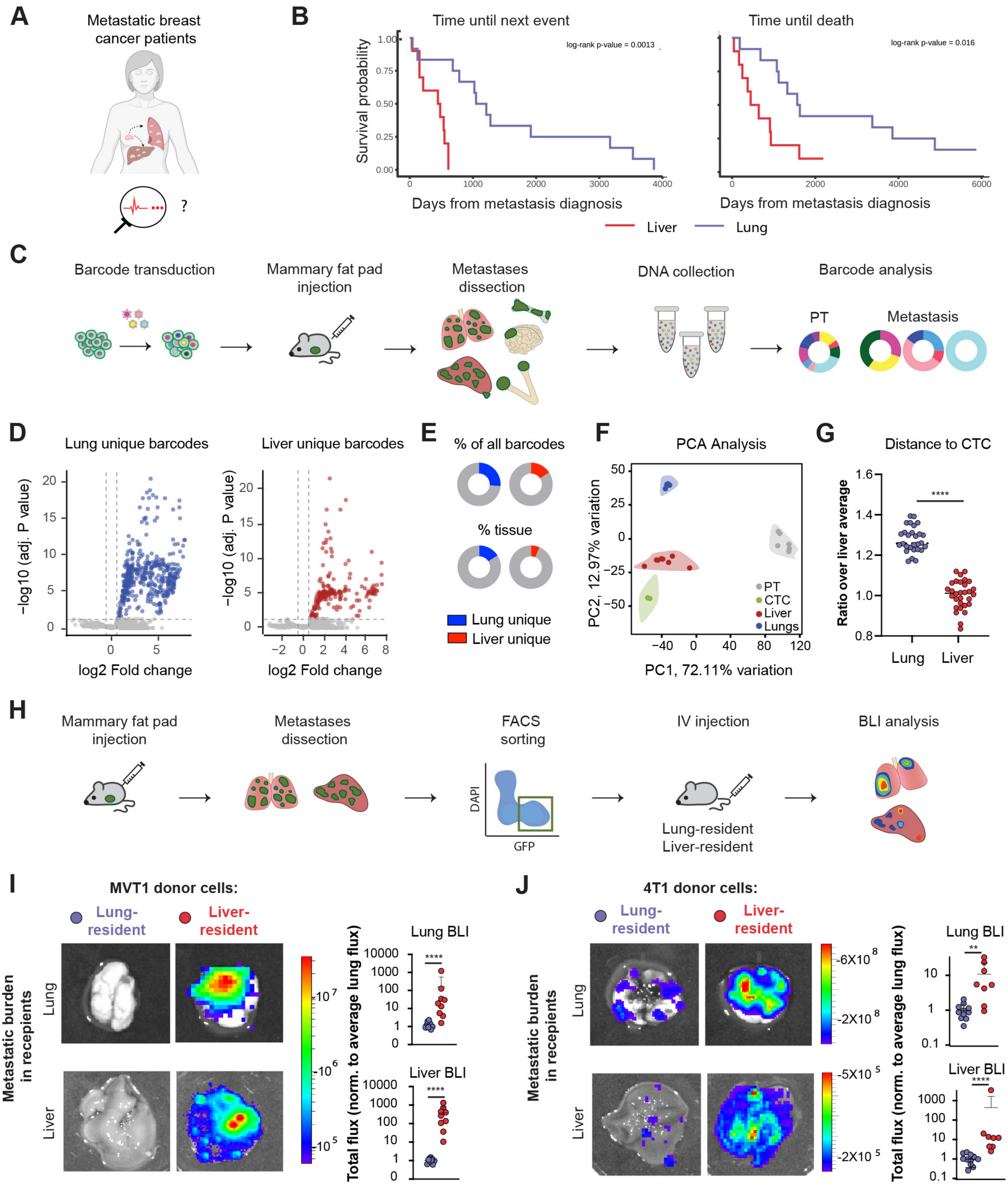

Figure 1. Metastatic ability of liver-resident versus lung-resident TNBC cells.
A. Schematic showcasing the concept behind patient data analysis. **B.** Kaplan-Meier plots depicting time to next metastasis or death (*left*) and overall survival (*right*) of breast cancer patients with the first mono-metastatic event detected in lungs (n=12) or liver (n=10). **C.** Schematic representing the experimental design for barcode labelling and metastasis clonality assessment in NSG mice carrying MVT1-GFP-luciferase tumors. **D.** Volcano plot illustrating unique barcodes for lung and liver metastases of a representative mouse. **E.** Pie charts showing the percent of unique barcodes detected in lungs or liver metastases (*top*), as well as the unique barcode contribution to metastasis in lungs and liver (*bottom*). **F.** Principal component analysis (PCA) plot of 500 top variable barcodes represented in the primary tumor (PT), circulating tumor cells (CTCs), lung and liver metastases of a representative mouse. **G.** Dot plot showing Euclidean distances measuring the dissimilarity in barcode expression between lung or liver metastases and CTCs (n=3mice). ****, $P < 0.0001$ by Mann-Whitney test. **H.** Illustration of the experimental design for metastatic potential assessment of lung- and liver-resident cancer cells. **I-J.** Representative images (*left*) and quantification (*right*) of bioluminescent signals in indicated organs of animals injected with lung- and liver-resident MVT1-GFP-luciferase (**I**, n=9 mice per group) and 4T1-GFP-luciferase cells (**J**, n=11,8 mice per lung-, liver-derived groups, respectively). **, $P < 0.01$ by Mann-Whitney test. IV, intravenous; BLI, bioluminescence imaging.

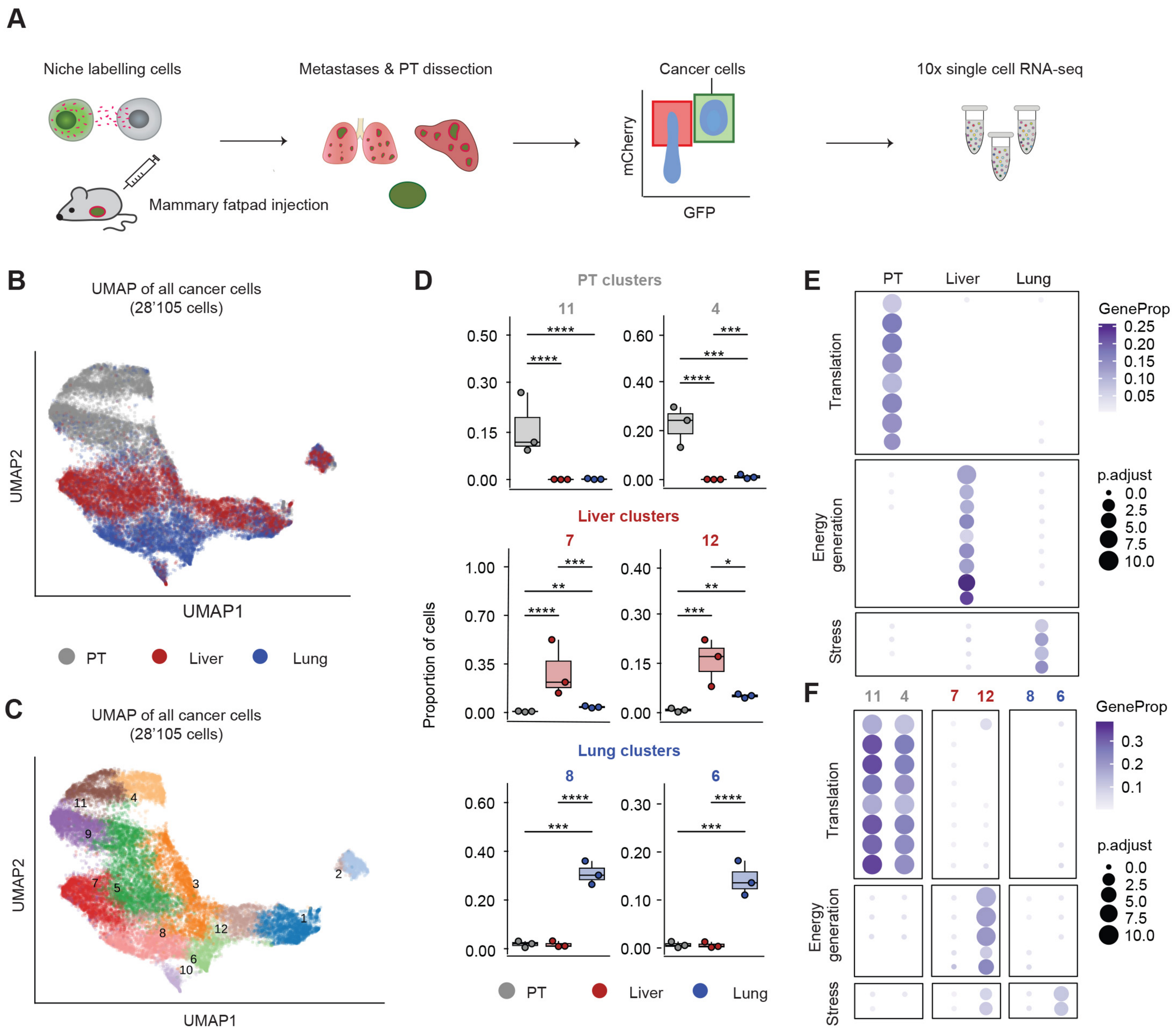

Figure 2. Liver-resident and lung-resident breast cancer cells display distinct molecular profiles.
A. Overview of the niche-labelling experiment with MVT1-GFP-luciferase xenografts with a specific focus on cancer cells. **B-C.** Uniform Manifold Approximation and Projection (UMAP) embedding colored by **B)** organ of origin and **C)** gene expression cluster number. **D.** Box-plot representation of specific gene expression clusters enriched within the primary tumor (PT), liver and lung metastases, along with associated abundances at each anatomical site (propeller derived adjusted *P* value; *, $P < 0.05$; **, $P < 0.01$; ***, $P < 0.001$; ****, $P < 0.0001$). **E-F.** Enriched reactome pathways in **E)** organ specific gene expression clusters and in **F)** all cancer cells associated with a given organ. Top 10 pathways for each group with hypergeometric test adjusted $P < 0.01$ are shown. Displayed is a condensed set of ontologies following simplification through semantic similarity. The complete pathway list is provided in tables S3 and S4.

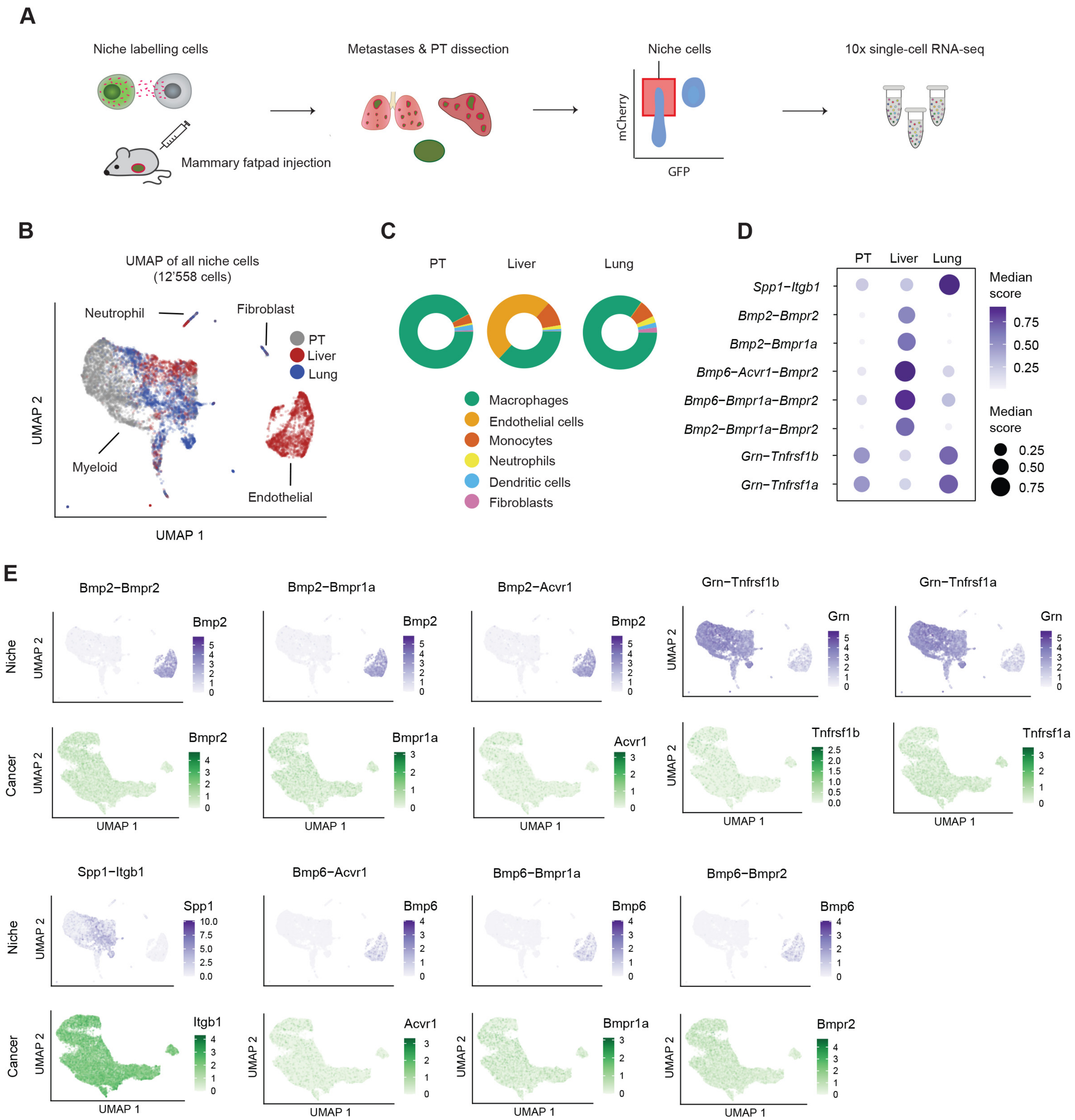

Figure 3. Metastatic niche composition of liver and lungs in TNBC.
A. Overview of the niche-labelling experiment with MVT1-GFP-luciferase transplants with a specific focus on metastatic niche cells. **B.** Uniform Manifold Approximation and Projection (UMAP) embedding of niche cells colored by organ. Annotations indicate the locations of estimated cell types within UMAP. **C.** Pie charts displaying cell type distributions within the primary tumor (PT) and the metastatic niches of liver and lungs. **D.** Dot plot representing selected interactions between cytokine ligands (niche cells) and their receptors (cancer cells). Dot color and size correspond to the average interaction score scaled for each ligand-receptor pair using minimum-maximum normalization. **E.** UMAP displaying cytokine and receptor expression in niche cells and cancer cells, respectively (refer to panel **B** and **Fig. 2B** for the cell type and organ of origin).

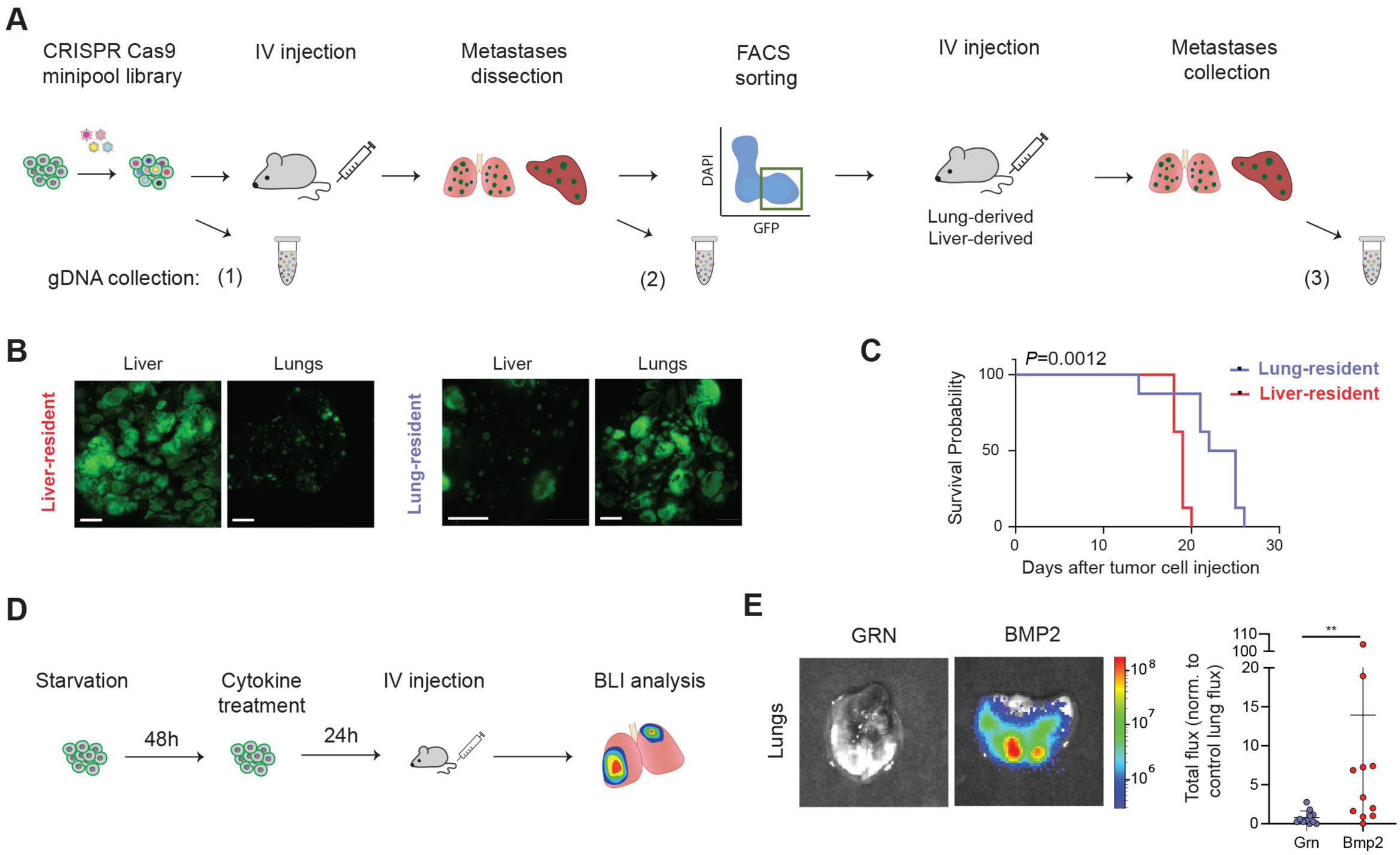

Figure 4. Niche-secreted cytokines impact on metastatic properties of lung-resident and liver-resident TNBC cells.
A. Illustration of the *in vivo* loss of function minipool CRISPR screen designed to investigate the role of selected cytokine-receptor pairs using MVT1-GFP-luciferase xenografts. **B.** Representative images of livers and lungs from animals re-transplanted with lung- or liver-resident cancer cells. GFP signal (*green*) demarcates the presences of cancer cells. Scale bars, 500µm. **C.** Kaplan-Meier curve showing the survival of mice re-injected with either lung- or liver-resident cancer cells. $P = 0.0012$ by log-rank test. **D.** Experimental design to explore the role of selected niche-specific cytokines in metastasis formation. **E.** Representative images (*left*) and quantification (*right*) of bioluminescence signals of lungs in animals injected with BMP2 and Granulin (GRN) treated cells. **, $P < 0.01$ by Mann-Whitney test. IV, intravenous; BLI, bioluminescence imaging.